Journal of Alloys and Compounds 1009 (2024) 176921



Contents lists available at ScienceDirect

Journal of Alloys and Compounds

journal homepage: www.elsevier.com/locate/jalcom



The structural and mechanical properties of open-cell aluminum foams: Dependency on porosity, pore size, and ceramic particle addition

Zafer Gölbaşı [a,*], Bülent Öztürk [a], Nuray Beköz Üllen [b]

[a] Department of Metallurgical and Materials Engineering, Karadeniz Technical University, Trabzon 61080, Türkiye
[b] Department of Metallurgical and Materials Engineering, Istanbul University-Cerrahpasa, Istanbul 34320, Türkiye

ARTICLE INFO

Keywords:
Open-cell aluminum foam
Porosity
Pore size
Ceramic particles
Mechanical properties

ABSTRACT

Aluminum foams are desired for lightweight, high-performance, and cost-effective materials, particularly in automotive, aerospace, and advanced power plants. Expansion of their applications depends on developing a detailed understanding of the structural and mechanical properties of aluminum foams. In this research, open-cell aluminum foams with 25.51–81.88 % porosity were manufactured through powder metallurgy using a space holder technique, with varying carbamide (urea) ratios (17–80 %) and particle sizes (1–1.4 mm, 1.7–2 mm, 2–2.4 mm). Three different ceramic particles, B_4C, Al_2O_3, and SiC were used as reinforcement to improve the compression properties and energy absorption capacity of the foam materials. The study determined open and closed porosity ratios, spherical diameter, sphericity values, micropore sizes, mechanical properties, and energy absorption capacity of the foam samples both with and without ceramic additives. The results show that porosity ratio, pore size, and ceramic particle addition significantly affect aluminum foams' structural and mechanical properties, allowing for tailored properties for specific applications. It was observed that as porosity increased, compressive stress decreased, and the length of the plateau region and the shape change where densification began increased. However, there was no significant change in compressive stress and specific energy values with changing pore size. The optimal B_4C addition was found to be 4 %, which significantly improved compressive strength to 3.75 MPa and specific energy to 4.24 MJ m^{-3}.

1. Introduction

Metallic foams are a new generation of materials with a lightweight structure and exceptional mechanical, electrical, thermal, and acoustic properties. With the development of technology, the importance of metallic foams with lightweight materials and high porosity has increased [1–4]. Metallic foams are classified into two groups: open and closed porous, based on the shape, size, anisotropic properties of the pores, and the state of contact between the cell walls. If the pores are separated from each other by a cell wall, it is called closed-pore metallic foam; if there is no cell wall between the pores and they are connected and continuous, it is called open-pore metallic foam. Open-cell metal foams possess unique properties such as low density, high specific surface area, sound and energy absorption, and excellent permeability, making them highly attractive for a wide range of applications. Because of these properties, metallic foams are used in various industries, such as automotive, space vehicles, defense, heat exchangers, cooling systems, etc. [5–8].

Metallic foams can be manufactured using many different methods, such as powder metallurgy, casting, polymer impregnation, gas injection into molten metal, foaming of molten metal by adding a foaming agent, etc. [9–12]. Open-cell metallic foams can be manufactured using the space holder method, which is one type of powder metallurgy technique. Different types of space holders are used in foam production including K_2CO_3 particles [13], sodium chloride (NaCl) particles [14], urea particles [15,16], saccharose [17], acrowax [18], ammonium bicarbonate [19], starch [20], camphene [21], PMMA [22], $MgSO_4$ [23], titanium particle [24], calcium chloride particle [25].

A variety of metals and their alloys, such as stainless steel, aluminum, titanium, copper, zinc, and magnesium are used in foam fabrication, each offering unique properties for specific applications [1,2,13,14,26–28]. Aluminum (Al) and its alloys have become widely used materials in foam production in recent years because of their low density, good corrosion resistance, and low melting temperature [29]. Noteworthy characteristics of these materials include their favorable mass-to-volume ratio, robust strength, excellent machinability, efficient

* Corresponding author.
E-mail address: zgolbasi@ktu.edu.tr (Z. Gölbaşı).

https://doi.org/10.1016/j.jallcom.2024.176921
Received 25 August 2024; Received in revised form 18 September 2024; Accepted 7 October 2024
Available online 9 October 2024
0925-8388/© 2024 Elsevier B.V. All rights are reserved, including those for text and data mining, AI training, and similar technologies.

thermal and electrical conductivity, and straightforward manufacturability. The superior properties of Al and its alloys have positioned them as crucial materials in the aerospace, automotive, and shipbuilding industries [2,30–32].

The mechanical properties of foams, like specific strength and modulus, compression behavior, and fatigue resistance are influenced by factors, such as cell topology (open or closed cell), cell size and shape, sintering conditions, and relative densities [33,34]. The cell shape significantly influences the design of foams customized for specific applications, because the mechanical properties are intricately linked to the geometry of the cells. Hassani et al. [35] produced aluminum open-cell foams with graded cell size and density using carbamide as space holders via powder metallurgy. The compressive properties of graded foams were compared to those of their non-graded counterparts. It was observed that the cell size-graded foam exhibited a wider plateau region in the stress-strain curve, higher densification strain, and greater energy absorption efficiency compared to the non-graded foam. In another study, aluminum foams with a maximum porosity of around 70 % were successfully produced through the powder metallurgy method known as the sintering and dissolution process. The optimal sintering temperature for producing Al foams with good metallurgical bonds was found to be 620 ºC. The sample with higher carbamide content showed the lowest yield stress value [36]. Jha and Mondal [26] created titanium foam with adjustable porosity (65–80 %) using NaCl particles through powder metallurgy. Variations in titanium content in the powder mixture impacted the relative density and cell wall thickness of the foam, while the yield stress and modulus of elasticity at different deformation rates varied between 12 and 30 MPa and 8–15 GPa, respectively. Sathaiah et al. investigated how space holder shape and type influence the mechanical and thermal properties of the foam. They utilized spherical carbamide and cubic sucrose as a space holder. Foams produced using spherical carbamide exhibited a threefold increase in mechanical properties compared to foams produced using cubic sucrose at the same equivalent relative density. Additionally, space holder shape (spherical or cubic) had no significant impact on heat conduction coefficient when pore rate and relative density values were consistent [2]. Hassanli et al. created aluminum foams of varying densities (0.28–0.48) using carbamide particles as space holders. They investigated how the structural design affected the mechanical properties. The results pointed out a twofold increase in plateau tension and a 75 % boost in energy absorption in foams of the same density. In the transition from uniform structures to layered structures, the energy absorption increased by 72 % at low densities and 15 % at high densities [37]. To improve the compression properties and energy absorption capacity of the foam materials, different ceramic particles, namely, B_4C, Al_2O_3, and SiC were used as reinforcement. Li et al. investigated the effects of B_4C ceramic particle addition on the mechanical properties and energy absorption of Al matrix composite and pure Al foam structures. As a result of the compression tests, the maximum compressive stress, modulus of elasticity, and toughness value of pure Al foams are 5.9 MPa, 5.9 GPa, and 10.9 MJ m^{-3}, respectively. It has also been found that the addition of ceramic particle reinforcement to the composition increases the mechanical properties [38]. In another study, Al matrix metallic foams with B_4C particles on 0.5–2.5 vol% using powder metallurgy-space holder method were created and structural and mechanical properties of the foam composites produced were investigated. The compression tests revealed a trend: mechanical properties decreased with increasing porosity, peaked at 2 % B_4C reinforcement, and then declined with 2.5 % B_4C. The even distribution of B_4C particles within the cell walls improved the strength of the material. Samples with 2 % B_4C reinforcement had a yield stress peak at 23.90 MPa and an energy dissipation capacity of 11.47 MJ m^{-3} [39]. Alizadeh and Mirzaei-Aliabadi [40] investigated the compressive properties and energy absorption behavior of Al–Al_2O_3 (0–10 vol%) composite foam, synthesized by the powder metallurgy-space holder method. The results indicated that the compressive properties were affected by reinforcing ratio and the composite foams containing 2 vol% Al_2O_3 displayed maximum compressive strength and energy absorption.

As noted above, the literature contains studies where aluminum foams with various porosities and pore sizes are used together. These studies generally investigated and discussed the effect of the foam production parameters namely foam generation pressure, sintering temperature, and sintering time, on the structural and mechanical properties. However, no specific studies have been found to investigate the influence of porosity, pore sizes, and the ratio and type of ceramic particles on the structural and energy absorption properties simultaneously. It is important to conduct further research on the structural and mechanical properties of aluminum foam materials for their large-scale usage. In light of these considerations, the current study aims to investigate the effect of porosity, pore size, and the ratio and type of the ceramic particle on the structural, compression properties, and energy absorption capacity of the open-cell aluminum foams with and without ceramic additives.

2. Experimental procedure

2.1. Material and foam production

Aluminum powder with 99.5 % purity and <44 μm size range was used in this study and purchased from Alfa Aesar Chemical Reagent Co. Technical grade carbamide (urea) was utilized as a space holder material due to its high solubility in water. The highly spherical carbamide (urea) particles supplied by Merck KGaA have a melting temperature of 133 °C, a density of 1.34 g $cm^{-3,}$ and a water solubility of more than 1000 g L^{-1} at 20 °C. Open-cell metallic foams were produced using a space holder technique through powder metallurgy at five different porosity levels and three different pore sizes. The porosity and pore size of the foams can be controlled by adjusting the volume and size of the space holder material used. For this purpose, in the sample production, spherical carbamide (urea) particles were utilized in different volume fractions of 17, 34, 51, 66, and 80, and sizes ranging from 1 mm to 1.4 mm, 1.7 mm to 2 mm, and 2 mm to 2.4 mm.

To evaluate the effect of the type and proportion of ceramic particles on the properties of the foam, B_4C was added to a mixture of carbamide and Al powder with a volume ratio of 66 % and a particle size range of 1.7–2 mm. B_4C ceramic particles, with a purity of 99.7 % and a size of less than 10 μm, were added to this mixture in different weight ratios of 1 %, 2 %, 4 %, 7 %, and 10 %. An optimal ratio was determined based on these weight ratios. Then, according to the optimum ratio, two different ceramic particles Al_2O_3 (99 % purity, <10μm) and SiC (99.9 % purity, <10μm) were used to produce foam materials. Subsequently, the structural and mechanical properties of the open-cell aluminum foams without and with ceramic additives were investigated.

The scanning electron microscope (SEM) images and particle size distributions of aluminum powder, Al_2O_3, B_4C, and SiC particles are depicted in Fig. 1. The image of carbamide particles is shown in Fig. 2.

The production of open-cell aluminum foam by space holder-water leaching technique in powder metallurgy involves four main stages: powder mixing, compaction, dissolving in water, and sintering. The manufacturing stages of the aluminum foams are shown in Fig. 3.

Initially, the surface of the carbamide particles was slightly moistened with ethanol so that they could be easily coated with aluminum powder. To achieve the desired porosities, carbamide as a space holder was added to the aluminum powders at varying volumes of 17 %, 34 %, 51 %, 66 %, and 80 %. The mixture was prepared by mixing in a turbila-type mixer at 57 rpm for 2 hours. Similar procedures were used for Al-ceramic particle composite samples. The powders were then compacted at 220 MPa using a uniaxial hydraulic press with a capacity of 60 tons into cylindrical specimens with a diameter of 20 mm and a length-to-diameter ratio of 1–1.2. The most critical step at this stage is to remove the carbamide without damaging the sample. Depending on the carbamide content of the samples, the water solubility times and the

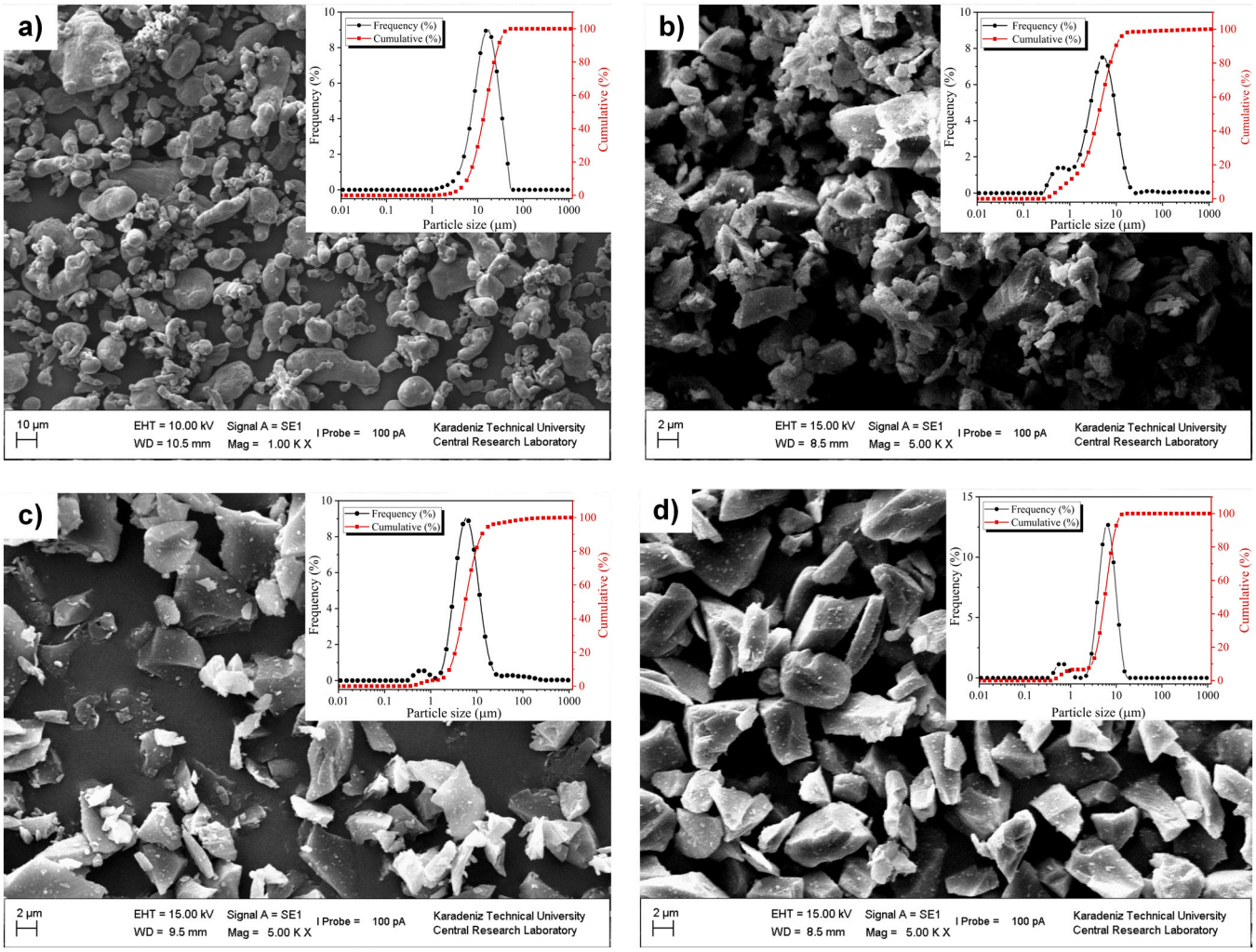

Fig. 1. SEM images and particle size distributions of raw materials: a) Al powder, b) Al_2O_3, c) B_4C, d) SiC particles.



Fig. 2. The image of the carbamide particles of different sizes.

amount of carbamide dissolved varied. After the carbamides in the structure were removed by soaking in pure water for 3–5 hours, the samples were first washed with ethyl alcohol and dried at 40°C for 2 hours and then at 60°C for 6 hours to remove moisture from the structure before sintering. All samples were sintered in a tube furnace (GSL-1500X) under atmospheric conditions at 630°C for 2 hours at a heating rate of 5°C min^{-1}. Following sintering, the aluminum foam samples were allowed to cool naturally in the furnace environment until room temperature before being removed.

A specific code system was established to identify the aluminum foams without and with ceramic additives to prevent confusion and duplication. The samples are assigned codes consisting of two numbers and a lowercase letter. The sequential position of each number and letter is crucial for identifying the metallic foam. The numbers in the codes, such as 17, 34, 51, 66, and 80, define the volume fraction of the carbamide used for foam production. The letters a, b, and c in the codes represent the particle size ranges of carbamides: 1–1.4 mm, 1.7–2 mm, and 2–2.4 mm, respectively. If there is in coding, the number in the 3rd row indicates the weight ratio of the ceramic particle added to the foam, and the capital letter in the 4th row illustrates the type of ceramic particle. The letters A, B, and S represent Al_2O_3, B_4C, and SiC, respectively.

2.2. Characterization methods

The densities of aluminum foams were determined according to the Archimedes Method using a Sartorius model CP2245-OCE digital balance and a density determination device with 1 mg precision. The volume and densities of the samples were calculated by measuring their weight in air and hexane. To determine the open and closed pore ratios, the samples were kept in paraffin boiling at 150°C for 1.5 hours, and the weight measurements of the samples were performed after the paraffin was impregnated into the pores. The volume change of 7.2 % during the melting of paraffin was accounted for in the calculations. Relative density was calculated by dividing the density of the foam material by 2.71 g cm^{-3}, which is accepted as a reference. The pore morphology of the open-cell aluminum foams with different pore ratios was examined using SEM (Zeiss EVO L10). The shape, size, and size distribution of the pores of the foams were determined using the commercial image analysis software Clemex Vision PE. The micropore sizes in the foams' structures after sintering were measured using the Quantachrome Poromaster PM 60 mercury porosimeter device according to the ASTM D 4404 standard. The post-sintering size measurements of the samples

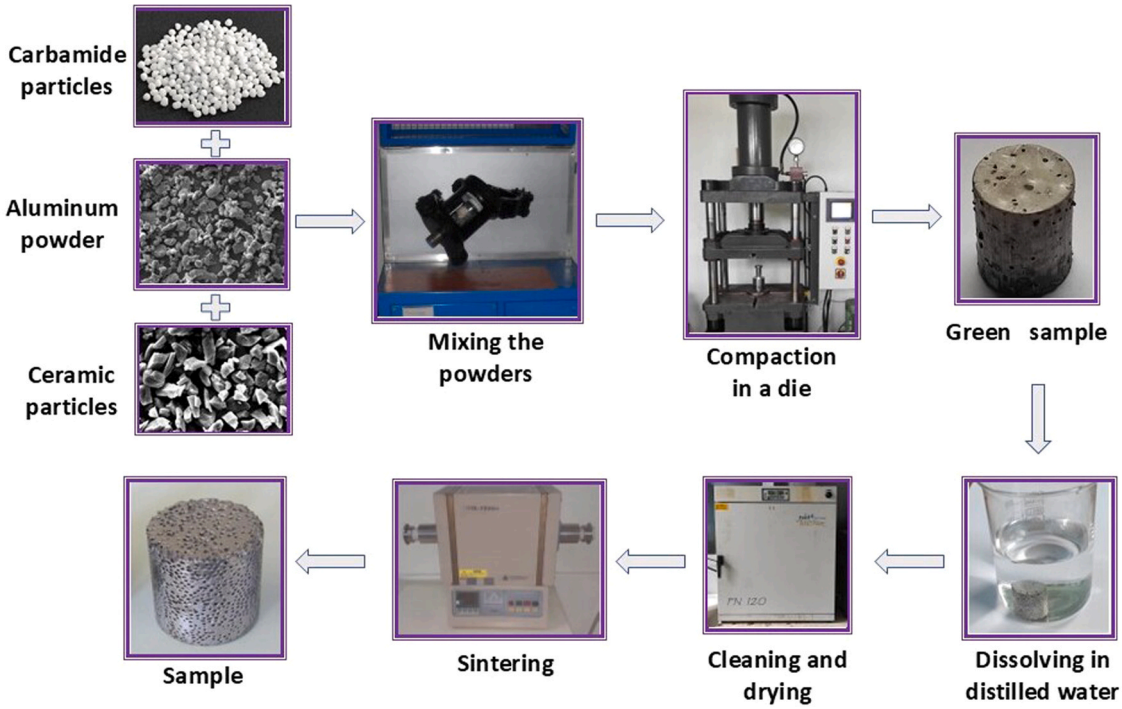

Fig. 3. Schematic representation of the open-cell aluminum foam fabrication process.

produced using carbamides with different percentage volume ratios were compared with the pre-sintering size measurements, and the volume changes in the samples were determined. Dimensional measurements of the samples after sintering were determined with an accuracy of 0.01 mm, and the resulting volume changes were calculated.

2.3. Mechanical tests

The compression tests of the aluminum foams were performed on an INSTRON brand 3382 model 100 kN capacity universal test device. The tests were conducted at room temperature with a crosshead speed of 0.85 mm min^{-1}. The Young's modulus of the Al foams was calculated using the slope of the elastic region, while the plateau stress was determined by measuring the distance from the yield point to the strain axis on the compressive stress-compressive strain curves. The compressive stress was calculated using the apparent cross-sectional area of each sample.

The energy absorption capacity is defined as the energy needed to deform a sample following specific deformations and serves as a metric for comparing foams with varying porosities [41,42]. The energy absorption properties of the foams involve evaluating their capacity to absorb energy (W). The amount of energy absorbed per unit volume was determined using Eq. (1) [30,43].

$$W = \int_0^{\varepsilon_m} \sigma(\varepsilon)d\varepsilon \quad (1)$$

In this context, W represents the energy absorption per unit volume, with ε_m denoting an arbitrary strain, σ representing stress, and ε indicating strain, where σ is a function of ε.

3. Results and discussions

3.1. Morphology of the Al foams

The macrostructures of foams with different porosity ratios are depicted in Fig. 4. The figure illustrates the presence of spherical and near-spherical pores formed by spherical carbamides. The

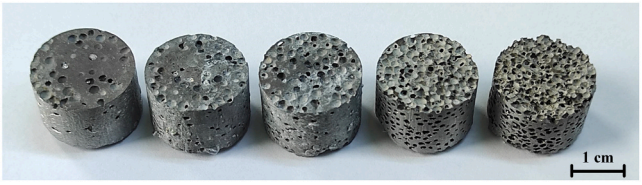

Fig. 4. Macrostructure of 17-b, 34-b, 51-b, 66-b, and 80-b coded foams.

interconnectedness of the cell walls of the carbamide added to the composition and its spherical shape indicates that it is distributed uniformly within the structure and the carbamides do not disintegrate.

Additionally, SEM images of the microstructures of the foams selected at different magnification ratios (50X, 1000X) are given in Fig. 5.

When evaluating the images in Figs. 4 and 5 together, it is seen that the pore morphology exhibits a behavior close to spherical and the pores are separated from each other by pore walls. The morphology of the pores after sintering is similar to the morphology of carbamide particles. This is clear evidence that pore structures can be designed by providing the appropriate properties of carbamide particles. Although the macropores seen in SEM images appear to be isolated from each other, they are connected by micropores in the cell walls. The foamy structures essentially contain two types of pores. The macropores are formed by removing the spacer from the environment while micropores are created in the cell walls during the pressing and sintering processes. Although macropores appear to be isolated from each other, they are connected by micropores in the cell walls. The interconnectedness of the pores has increased with increasing porosity. Additionally, it is seen in the SEM images in Fig. 5 that the porosity increases with increasing carbamide content, and the number of cell walls increases accordingly. It was observed that the pore size and ratio of the sintered samples can be controlled by adjusting the amount and the size of the carbamide used. Moreover, in the cross-section parallel to the pressing direction, relatively elliptical pores were observed along with spherical pores. The possible reason is that the spherical carbamide particles change their

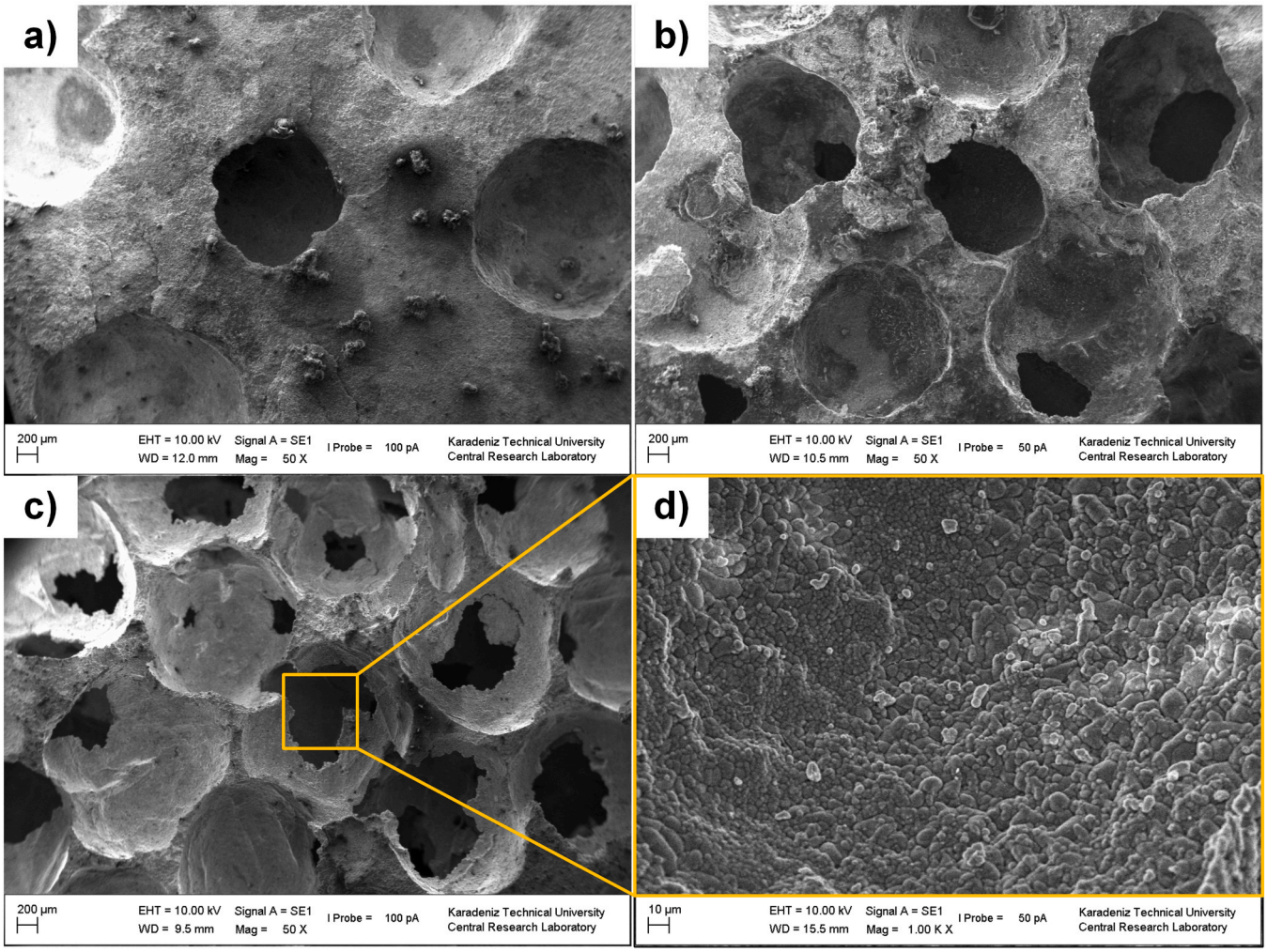

Fig. 5. SEM images of metallic foam coded as a)17-b, b)51-b, c)80-b, and d) higher magnified view of 80-b.

original shape and become flat along the compression direction during compression [44]. Sathaiah found that as the amount of carbamide increased, the porosity ratio and the number of open pores also increased. The cell wall thickness decreased with increasing porosity. Foams with high porosity have increased pore openness and decreased cell wall thickness with increasing porosity due to more effective contact with each of the space holders with decreasing aluminum content [1,2,19]. Microporosity is influenced by the powder metallurgy method, while macroporosity is influenced by the type of carbamide used as a spacer [45]. Samples with high porosity were produced using the powder metallurgy method by incorporating carbamide in various ratios, sizes, and shapes. It was shown that the porosity, size, and shape of these samples can be controlled by adjusting the amount, particle size, and shape of the space holder used [1,2,36,45,46].

3.2. Densities and porosity levels of the Al foams

Density can be controlled by varying parameters such as total, open, and closed porosity, carbamide particle size, and amount. Table 1 presents density, relative density, total porosity, and the open and closed porosity ratios of foams produced using three different sizes of carbamide and different ceramic particles.

As seen in Table 1, the density, and open and closed porosity of the samples range between 0.48 and 2.01 g cm^{-3}, 17.15–65.12 %, and 6.14–19.73 %, respectively. The total porosity of the samples consists of between 25.51 % and 81.88 %. Open, closed, and total porosity ratios of

Table 1
Density, relative density, total porosity, open and closed porosity ratios of the samples.

Sample code	Density (g cm^{-3})	Relative density	Total porosity (%)	Open porosity (%)	Closed porosity (%)
17-a	1.98	0.73	26.47	17.15	9.32
17-b	2.01	0.74	25.51	18.57	6.94
17-c	1.98	0.73	26.44	18.96	7.48
34-a	1.46	0.54	45.62	36.25	9.37
34-b	1.42	0.52	47.17	37.26	9.91
34-c	1.50	0.55	44.40	38.26	6.14
51-a	1.10	0.41	59.06	45.25	13.81
51-b	1.12	0.41	58.36	46.89	11.47
51-c	1.02	0.38	62.06	44.66	17.36
66-a	0.86	0.32	67.95	55.26	12.69
66-b	0.88	0.32	67.32	58.66	8.66
66-c	0.89	0.33	66.95	53.25	13.70
80-a	0.48	0.18	81.88	62.15	19.73
80-b	0.51	0.19	81.06	65.12	15.94
80-c	0.51	0.19	80.92	64.12	16.80
66-b–1-B	0.82	0.30	69.32	57.25	12.07
66-b–2-B	0.86	0.32	68.06	59.25	8.81
66-b–4-B	0.78	0.29	70.88	55.25	15.63
66-b–7-B	0.86	0.32	67.95	55.15	12.80
66-b–10-B	0.86	0.32	67.95	59.15	8.80
66-b–4-A	0.80	0.29	69.48	56.28	13.20
66-b–4-S	0.82	0.30	70.16	55.12	15.04

samples with ceramic additives were found to be approximately equal to those of the samples without ceramic additives. This leads to the conclusion that adding ceramic particles to foam samples does not significantly affect pore formation. Since the shrinkage during sintering is inversely proportional to the raw density, samples with higher amounts of carbamide have lower raw density and are relatively denser after sintering. It was found that the open pore ratios and total pore ratios increased with increasing carbamide content due to the interconnection of the pores [2,45,47]. There are similar results in the literature. Aida produced foams with a density of 0.57–0.61 g cm^{-3} and a total porosity of 64.7–67.3 % using Mg powders containing 50 wt% carbamide [15]. Beköz reported that the open, closed, and total pore rates of Astaloy Mo varied between 23.8 % and 68.4 %, 2.6–27.1 %, and 49.2±1.7–71.0±2.1 %, respectively [48]. Bafti found that the porosity levels of aluminum foams produced using 60 wt% carbamide as a spacer were within the range of 40–85 % [43]. Controlling the total porosity and pore size distribution in a porous structure is key to materials required for specific applications.

3.3. Volume changes and micropore sizes in foams

When using carbamide in the range of 17–80 % by volume, regardless of the pore former diameter, the average volume changes in the samples after sintering were determined as 1.7 %, 2.3 %, 2.5 %, 3.1 %, and 4 % respectively, with increasing carbamide content. Volumetric shrinkage of the samples is also due to shrinkage during sintering. Before sintering, volumetric shrinkage is lower because the densities of samples with lower carbamide content and fewer pores are higher than those with higher pore content. As the amount of porosity increases, the amount of volumetric shrinkage also increases. After sintering, all samples showed a volume change, and the amount of volume change increased with the increase in carbamide ratio due to the increase in porosity ratio. Experimental results indicate that increasing the carbamide content leads to larger and more numerous macropores, while the similar properties of micropores decrease. This increase improves densification during the compression of powder mixtures through plastic deformation due to its softer nature. As porosity increases and density decreases, volume shrinkage increases due to increased sintering shrinkage [49]. Manonukul et al. found that volume shrinkage increased with increasing space holder content in stainless steel foams [50].

The maximum pore sizes after sintering were found to be 98 μm, 127 μm, and 118 μm, respectively, depending on the carbamide size used between 1 and 1.4 mm, 1.7–2 mm, and 2–2.4 mm. The maximum pore size determined serves as the upper limit for micropore dimensions within the pore walls of the resulting porous sample. It was observed that the pore sizes fell within the range of pore values reported in the literature (75–172 μm), albeit at varying rates [51,52].

3.4. Spherical diameter and sphericity distributions of macropores

Image analyzer software was used to determine the pore size (spherical diameter) and pore shape (sphericity) from SEM images of the foams created with carbamides of various particle sizes and volume ratios. The mean spherical diameter and the mean sphericity of the macropores were calculated and are provided in Table 2 for comparison purposes.

In Table 2, the maximum spherical diameter, average spherical diameter, and average sphericity values of the samples are in the range of 872.5–1298.5 μm, 469.5–982.8 μm and 0.55–0.84, respectively. An increase in carbamide content initially leads to an increase and then a decrease in sphericity. The average sphericity decreased with increasing pore ratio due to the increase in inter-pore connectivity. The decrease in sphericity and size may be due to the comminution of carbamide during both the wetting and pressing processes. The interconnection of larger pores as the pore ratio increased also led to an increase in pore size. The results indicate that the average sphericity and spherical diameter values of macropores change according to the dimensional properties of the spacer.

When the particle size of urea is 1.0–1.4 mm, 1.7–2.0 mm, and 2.0–2.4 mm, the average pore size of the aluminum foam longitudinal section is 681.6 μm, 602.92 μm and 748.64 μm, respectively. Mutlu et al. produced samples with an average spherical diameter of 607 μm and a sphericity distribution in the range of 0.56–0.62 using Ancorstell 4300 steel powder (Cr-Sr-Ni-Mo) and irregularly shaped carbamides with a particle size range of +710–1000 μm [53].

With an increasing carbamide ratio (from 17 to 80), the increase in porosity increased the average pore size. The reason why the maximum pore size is larger than the size of the spacer used is that macropores connect, creating larger pores in volume [48,54]. While the pores were connected in samples produced using high amounts of carbamide, pore connections decreased as the amount of carbamide decreased. This situation caused changes in the pore ratios and spherical diameter-sphericity values of the pores in sintered samples [55].

Table 2
Spherical diameter and sphericity distributions of the samples.

Sample Code	Spherical diameter (μm)				Sphericity			
	Minimum	Maximum	Average	Standard Deviation	Minimum	Maximum	Average	Standard Deviation
17-a	466.3	962.8	752.6	169.8	0.29	0.97	0.71	0.167
17-b	533.6	1026.2	608.7	196.5	0.41	0.99	0.79	0.253
17-c	673.3	1157.3	982.8	154.3	0.11	0.98	0.73	0.223
34-a	241.5	1115.6	769.2	192.2	0.38	0.99	0.68	0.163
34-b	386.3	945.6	682.4	169.8	0.42	0.97	0.64	0.248
34-c	232.4	1298.5	852.2	173.4	0.18	0.99	0.66	0.173
51-a	223.6	1226.2	708.7	196.5	0.21	0.98	0.68	0.238
51-b	85.3	992.3	583.5	169.2	0.52	1.00	0.84	0.141
51-c	16.9	1083.7	756.3	172.8	0.33	1.00	0.72	0.256
66-a	66.6	996.2	608.7	196.5	0.21	0.97	0.61	0.238
66-b	52.5	1010.8	632.7	172.6	0.40	0.98	0.63	0.241
66-b−4-A	27.8	952.8	625.3	178.5	0.36	1.00	0.65	0.229
66-b−4-B	41.5	913.5	629.7	181.3	0.37	1.00	0.68	0.213
66-b−4-S	32.6	986.1	603.7	159.1	0.39	0.99	0.71	0.243
66-c	16.3	1045.6	682.4	169.8	0.38	1.00	0.72	0.253
80-a	169.2	986.4	569.2	165.3	0.18	0.95	0.55	0.223
80-b	112.8	913.5	507.3	160.1	0.19	0.93	0.57	0.228
80-c	70.3	872.5	469.5	167.4	0.11	0.91	0.56	0.223

3.5. Compressive behavior of open-cell aluminum foams

3.5.1. Effect of pore size

In this study, open-cell aluminum foams with different pore ratios were fabricated using carbamides with particle sizes ranging from 1 to 1.4 mm, 1.7–2 mm, and 2–2.4 mm in various proportions. Static deformation tests were carried out on foams with different porosity ratios, and the obtained compressive stress-strain graphs are given in Fig. 6

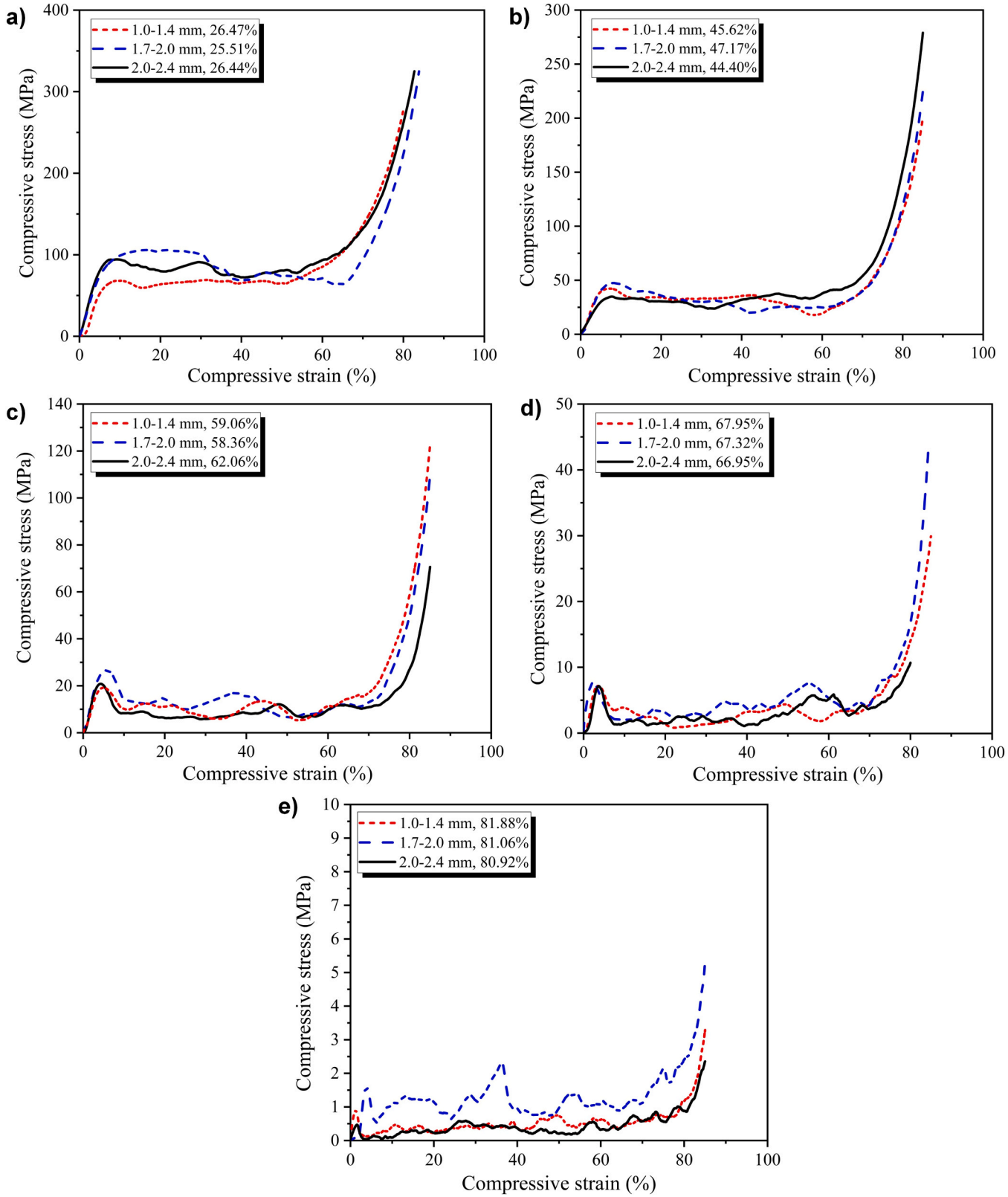

Fig. 6. Compressive stress-compressive strain curves of open-cell aluminum foams with porosities of a) 25.51–26.47 %, b) 44.40–47.17 %, c) 58.36–62.06 %, d) 66.95–67.95 %, and e) 80.92–81.88 %.

(a-e).

The compression curves in Fig. 6 display the mechanical behavior of typical porous materials. As can be seen from the graphs, at the beginning of deformation, compressive stress and compressive strain increase at a rate close to linear. In this region, known as the elastic deformation zone, elastic deformation occurs as a result of the bending of the pore walls, and stress rises linearly with strain at low stresses. There is a sharp decrease in stress in porous materials that exhibit brittle behavior due to fracture (breaking of the pore walls) that occurs after the elastic region. The stress at which this decrease occurs is called the upper yield stress or maximum compressive stress. In the next stage, there is a region where the stress partially changes at high deformations and plastic deformation occurs to a large extent. In this region, called the plateau region, sharp, dispersed, and non-symmetrical sudden ups and downs in stress occur as a result of the separation of the pore walls into layers during deformation. The plastic deformation and the fracture of cell wall are progressed simultaneously. With increasing porosity, open-pore structures deform primarily due to the bending of cell corners. At this stage, the formation of the plateau region, where deformation occurs at approximately constant stress, is associated with the collapse of the pore walls. Long plateau regions are a condition caused by open cellular morphology. In the final stage, as a result of the closure of the pores, the crushing of the pore walls, and their contact with each other, a region is formed where the stress increases rapidly and the deformation remains constant, as in dense materials. In this region, known as the densification zone, the compressive stress increases rapidly after the deformation rates vary according to the porosity ratio. Aluminum foams deform like a solid material and due to the brittle behavior of the foams, fracture occurs throughout at the end of the experiment. When all pores are closed, the pore walls come into contact with each other and act like a dense material, creating a region where stress increases rapidly. The densification stress changes the compressive strengths significantly. Initially increasing stress with decreasing pore size then tends to decrease. Metal foams exhibit a crucial characteristic in their capacity to absorb energy, with a substantial portion of the absorbed energy undergoing irreversible conversion into plastic deformation energy. This transformation predominantly occurs at elevated plateau stress levels, contributing significantly to a heightened energy absorption capacity. During the plateau stress phase, the foam experiences extensive energy absorption due to the bending and collapse of its cell walls. Once this mechanism concludes, stress rises, transforming the foam into a denser material. In contrast, solid parts demonstrate inferior performance in this aspect. Generally, a notable enhancement in energy absorption is observed with a shift in foam porosity levels from low to high. The interconnections of macropores increase with increasing porosity, and the structure caused by this situation tends to be weaker under compressive load.

As the pore ratio increases, the maximum compressive stress and plateau stress decrease, while the length of the plateau region (the change in shape at which densification begins) increases. Whether the pores are open or closed affects the length of the plateau area [2,45,48,56]. In all samples shown in Fig. 6a–e, with the increase in pore content, the maximum compressive stress decreased, and the length of the plateau region and the shape change at the place where condensation started increased. However, with the increase in carbamide content, the change in carbamide size did not have much effect on the compression behavior. Especially at an average porosity of approximately 81 % (see Fig. 6e), the shape changes where condensation begins is not significant. This can be explained by the rapid and uncontrolled breakage of the walls due to the dense pore rate. Although the yield stress is quite different at an average porosity of approximately 46 % and 60 % (see Fig. 6b and c), the length of the plateau region and the shape changes at the beginning of densification are similar. As the carbamide ratio increased, the porosity ratio also increased and at lower force values, the cell walls broke and moved towards the concentration areas. When the compressive stress-compressive rate curves are examined, it is understood that the fracture during the compression test is brittle [57].

The effect of the change in carbamide size on compressive stresses was evident at the 34 % carbamide usage rate by volume. Similar values were observed in terms of compressive stress and plateau stress when carbamides with particle size ranges of 1–1.4 mm and 1.7–2 mm were used. When carbamides with a particle size range of 2–2.4 mm were used, the maximum compressive stress and plateau stress decreased, while the length of the plateau region and the length of the region where condensation started increased. With increasing carbamide content (66 % and 80 % by volume), the pore walls collapse due to the increased pore content and the pore walls collide with each other and disperse. The connections between Al particles tend to be as weak as possible with increasing the porosity, and final strength of the foam decreased consequently. This situation manifests itself with a zigzag in the compressive stress-compressive rate curves. In specimens with high porosity, inhomogeneity of pore distribution and weakness of cell walls may cause brittle fracture. During the compression test, macropores in the structure create a notch effect, causing crack propagation and breakage of the material.

Within this study, since aluminum foams are produced in a relatively wide range of densities and properties, it is necessary to define which foam is most suitable in terms of energy absorption. Energy absorption, defined as the energy taken in per unit volume of a specimen under compression to a specified strain, is geometrically represented by the area beneath the stress-strain curve. This metric is essential for assessing the effectiveness of metal foams in absorbing energy during compression deformation. The absorbed energy is mostly converted into plastic deformation energy, which happens in the long plateau stress region and results in high energy absorption. As the cell walls gradually break and crush, the energy absorption increases. Eventually, the foamy structure behaves like a dense material. The dominant deformation mechanism is the buckling of cell walls during loading. This leads to the disruption of cell walls due to the initiation of cracks that propagate along the cell walls and cause fracture.

The macro images in Fig. 7 clearly show the three distinct regions of the stress-strain curve during the deformation test of aluminum foams: the elastic deformation region, the plateau region, and the densification region.

The plateau stress and energy absorption capacity of open-cell aluminum foams with different porosity ratios obtained from the compressive stress-compressive strain graphs are given in Table 3.

The energy absorption value of aluminum foams is lower in the elastic-plastic stage (Fig. 6). This is because the energy absorption of aluminum foams primarily occurs in the plateau stage due to the collapse of the pore structure. As porosity decreases, the energy absorption value increases with strain in a power function manner. This is due to the significant strain hardening effect of the aluminum foam and the increased plastic modulus when porosity is low. As the aluminum foam reached the point of densification stress, the stress increased, leading to a significant increase in energy absorption value. The energy absorption capacity depends on the length of the plateau region during compression, which can be controlled by the relative density, size distribution of pores, cellular morphology, and reinforcing particles. Bafti determined the average plateau stress values of the aluminum-based metallic foams it produced using 45 % carbamide by weight as 4–5.5 MPa. The average plateau stress of metallic foams coded 51-a, 51-b, and 51-c, with approximately the same porosity ratio, was determined as 9.49–12.37 MPa, which is approximately twice the average plateau stress in Bafti's study [45].

The specific energy value of the open-cell aluminum foam with 46 % porosity was determined as 20.93–21.87 MJ mm^{-3}, and the specific energy value of the metallic foam with 81 % porosity was determined as 0.35–0.84 MJ mm^{-3}. Specific energy values decreased with increasing porosity. In the study conducted by Sathaiah, the specific energy value of aluminum foam with 51 % porosity was determined as 3±0.45 MJ mm^{-3} [2]. In another study, Bafti obtained a specific energy value of 2.8 MJ m^{-3} in a 45 wt% carbamide metallic foam in the same particle size

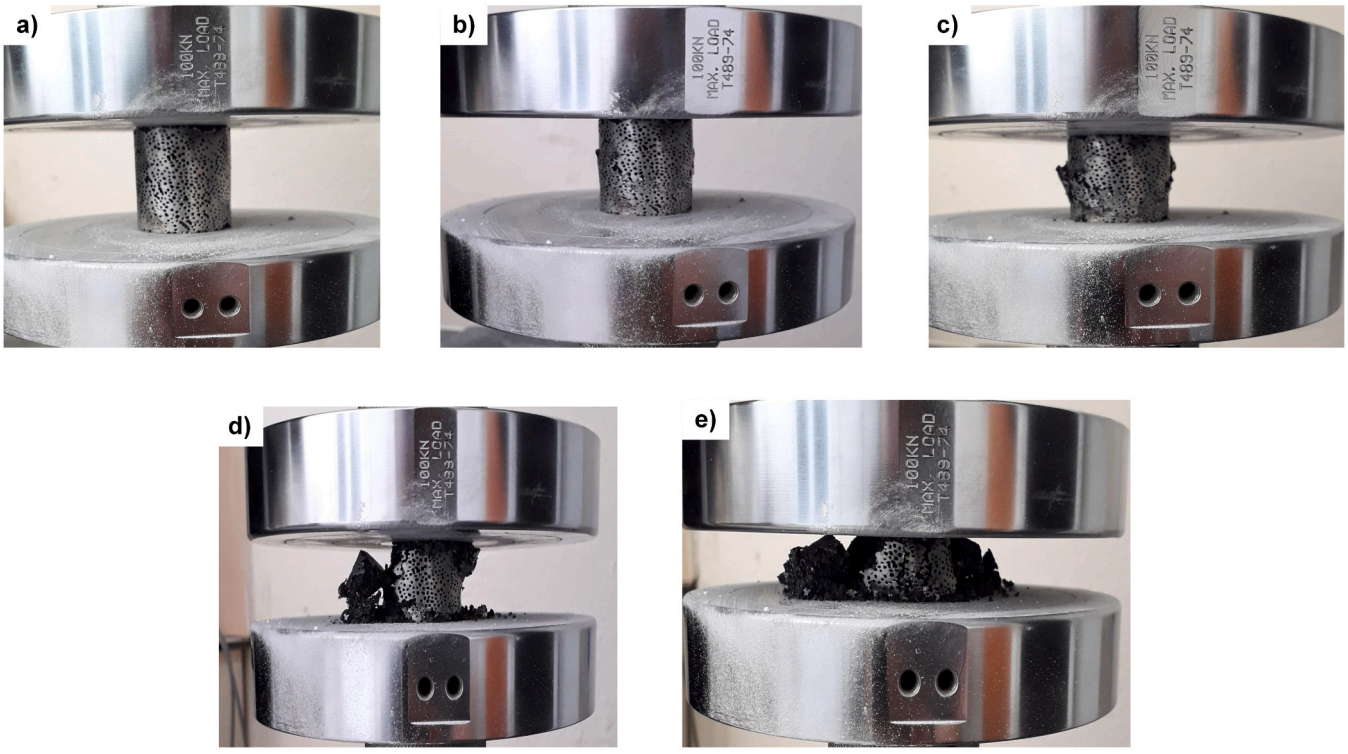

Fig. 7. Macro images of aluminum foams at different deformation rates a) 0 %, b) 15 %, c) 25 %, d) 45 %, and e) 65 %.

Table 3
The plateau stress and energy absorption capacity of open-cell aluminum foams.

Sample code	Plateau stress (MPa)	Energy (J)	Specific energy (MJ m^{-3})
17-a	67.13	284.74	51.80
17-b	74.18	317.72	57.76
17-c	72.67	295.75	53.80
34-a	34.08	126.74	21.19
34-b	29.94	125.21	20.93
34-c	33.63	130.84	21.87
51-a	9.49	38.81	7.23
51-b	12.37	56.58	10.55
51-c	8.18	40.12	7.48
66-a	2.91	13.44	2.28
66-b	3.75	18.27	3.09
66-c	2.08	17.12	2.90
80-a	0.43	2.18	0.35
80-b	1.01	5.17	0.84
80-c	0.33	2.40	0.39

range [45]. The decrease in compressive stress with increasing carbamide content is also observed in studies on stainless steel, nickel, and titanium samples [36,42,58].

The energy absorption capacity of foams with the 1.7–2 mm size range is higher than those with the 1–1.4 mm and 2–2.4 mm size ranges, and they can absorb more energy (Table 3). Therefore, carbamides in the 1.7–2 mm size range were used in the later stages of the study.

The model proposed by Gibson and Ashby is the most commonly used model to understand the mechanical properties of porous materials. According to this model, there are certain assumptions: (i) the walls of the pores forming the structure are dense material, (i) the strength of the porous material is linearly dependent on the relative density (ρ/ρ_s), and (iii) the contribution of the cell edge bending is assumed to be nonlinear. The Eq. (2) determining the Gibson and Ashby model is given below [59].

$$\sigma_y = \sigma_{ys} C \rho_{rel}^{3/2} \left(1 + \rho_{rel}^{1/2}\right) \quad (2)$$

where σ_{ys} is the yield strength of the bulk material, σ_y is the yield strength of the foam, ρ_{rel} is the relative density, and C (taken as 0.23) is a constant. The compression test results obtained in this study are compared with the Gibson and Ashby model in Fig. 8, according to the relative density and carbamide size. According to the values taken from the Handbook of Aluminum, the compressive yield strength of bulk aluminum is 200 MPa and its density is 2.71 g cm^{-3} [60].

When Fig. 8 is examined; it is seen that the compressive yield strength depends on the relative density and increases with increasing relative density. It is seen that the yield strength results exceed the model with increasing carbamide sizes. It occurs significantly above the relative density of approximately 0.40, below which the results fall

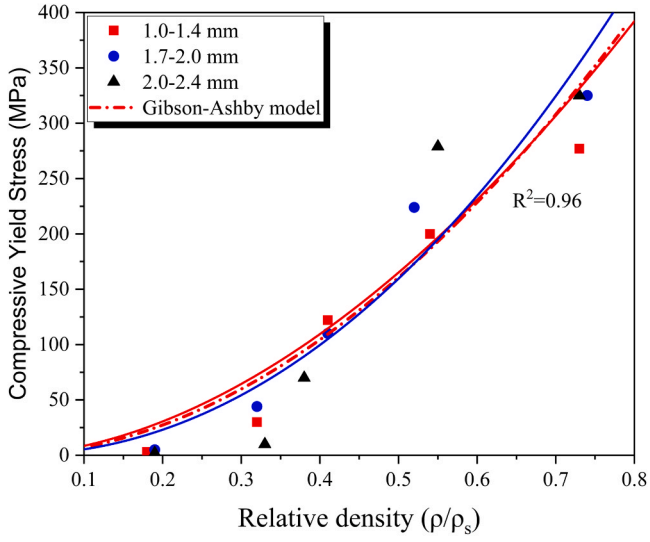

Fig. 8. Relationship between relative density and compressive yield stress of open-cell aluminum foam.

below the model. This situation can be explained by the increasing pore wall thickness. With increasing pore ratio, defects such as broken walls, larger pores, anisotropic pore structure, and irregular foam density and micropores in cell walls significantly reduce the mechanical properties of cellular solids. Beköz and Oktay reported that with increasing pore ratio, stress concentration occurs easily at the sharp edges of irregular pores and causes lower strength [48]. Sharma et al. stated that open-cell aluminum foams with high porosity exhibit higher normal stress and increasing stress plateaus under the same load. They also reported that increasing porosity causes an increase in compressive stresses and that supports the exhibit of complex stress fields [61].

The Young's modulus of aluminum foams was found to be 0.68–1.08 GPa, 0.45–0.66 GPa, 0.39–0.48 GPa, 0.19–0.32 GPa, and 0.03–0.07 GPa, respectively, with increasing carbamide content by volume. The modulus decreased with increasing porosity ratio. It can be clearly stated that most properties depend largely on the density of the foam structure and the properties of the matrix material.

3.5.2. *Determination of optimum additive ratio and additive type in ceramic particles added foams*

By adding 1 %, 2 %, 4 %, 7 %, and 10 % B_4C by weight to the starting aluminum powder, the effect of ceramic particle additive on the mechanical properties of metallic foams was examined and the optimum additive ratio was determined. The effects of B_4C addition on mechanical properties is given in Fig. 9.

As seen in Fig. 9, compressive stress values increased towards 4 % B_4C and then decreased. Thus, the optimum value is determined as 4 %. The mechanical properties of the 66-b-4-B of coded samples are higher than those of the other B_4C-added foams, and this is also seen in the specific energy values given in Fig. 10.

When specific energy values are compared; the specific energy value of the sample coded 66-b-4-B is 4.24 MJ m^{-3} and is higher than the energy values of other samples. The boron oxide layer surrounding B_4C particles promotes wetting due to the compatibility between the Al matrix and B_4C, thus enhancing strength. This situation is also seen in a similar study [62]. In addition, the increase in the rate of B_4C trapped in the pore walls causes the micropore ratio to increase due to it being a discontinuous phase [63].

The distribution of B_4C in the structure of the foams obtained by using B_4C at different ratios by weight (2 %, 4 %, 10 %) is given in Fig. 11. The black contrasting points in the microstructure represent B_4C.

Compression tests were performed on open-cell aluminum foams by adding at a rate of 4 % aluminum oxide (Al_2O_3) and silicon carbide (SiC) powders for comparison with foams without additives and B_4C additive foam, and the results obtained are given in Fig. 12.

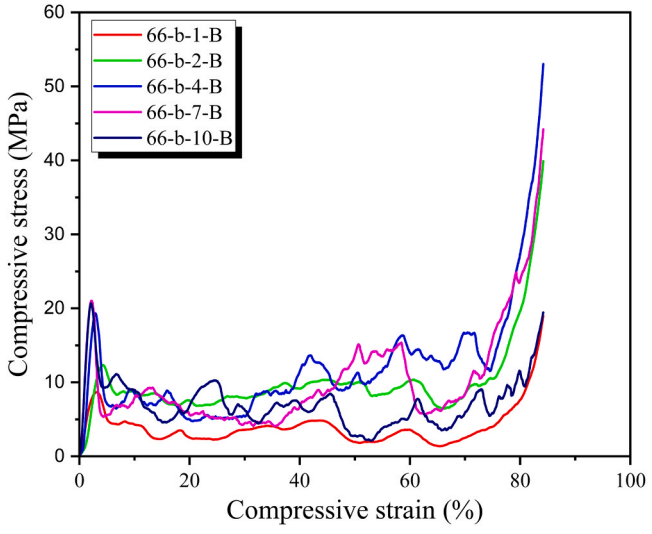

Fig. 9. Compressive stress-compressive strain graphs of B_4C added open-cell aluminum foam at different rates.

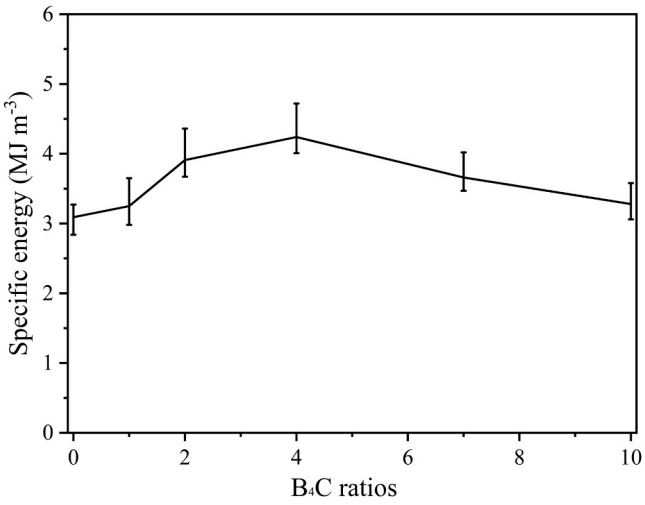

Fig. 10. Specific energy values of 66-b and B_4C additives open-cell aluminum foam.

As observed in Fig. 12, only the addition of B_4C increased the stress and energy values when compared. The ceramic particle added to the structure have either dispersed homogeneously within the foam or clustered together in clumps. As a result, while B_4C has increased the strength values, it has reduced the strength values of Al_2O_3 and SiC. This phenomenon, where the addition of B_4C ceramic particles increases the compressive stress in the structure, has also been observed in similar studies [39,64–66]. Restricting dislocation movements by adding ceramic particles into aluminum is another factor that increases strength. As dislocations move between particles, a ring of dislocations forms around the reinforcing particles. Each dislocation moving in the slip plane adds a ring around the particles, causing the dislocation density to increase. These dislocation rings cause internal stresses and thus deformation hardening of the aluminum phase. As a result, the strength of the material increases [57,67].

Table 4 summarizes some scientific studies investigating the properties of aluminum-based metallic foams with varying porosity produced using the powder metallurgy method.

4. Conclusions

The study examined the effect of carbamide ratio and size on the mechanical properties of open-cell aluminum metallic foams. Additionally, it determined the influence of the ratio and types of ceramic particles. The results can be summarized as follows:

- Compression tests and metallographic examinations revealed that the fracture was brittle.
- By adjusting the amount and particle size of the carbamide space holder, the pore size and ratio of the foams were effectively controlled, with post-sintering pore sizes recorded as 98 μm, 127 μm, and 118 μm, depending on the initial carbamide size.
- The porosity is directly related to the ratio of carbamide added, and the pore shape resembles the carbamide particle shape. Sphericity initially increased and then decreased with the increasing amount of carbamide.
- The compression test results were mainly characterized by three stages: a short linear stage, a long yield plateau stage, and a densification stage. The compressive strength values increased with decreasing porosity, while the densification strain decreased.

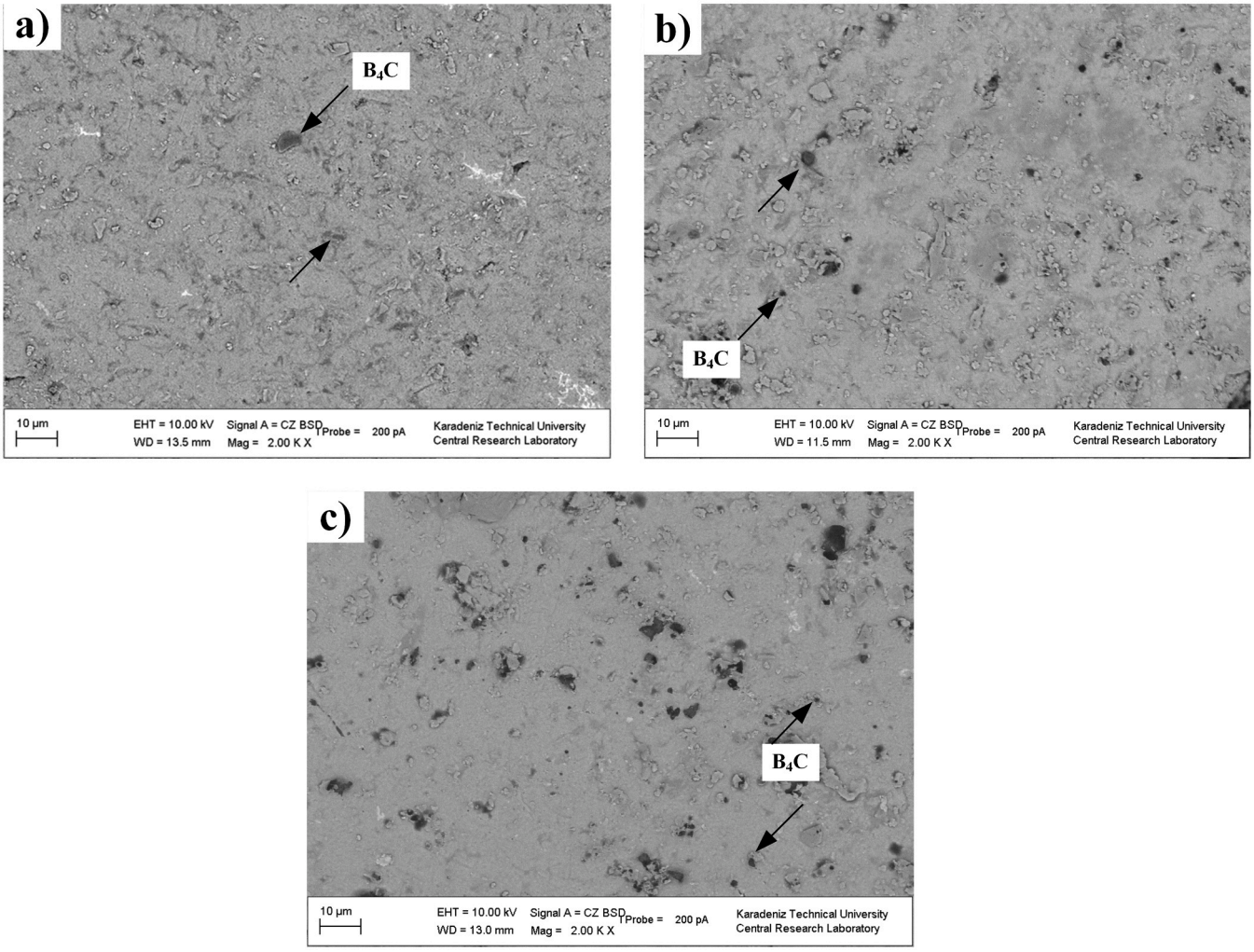

Fig. 11. Structural distribution of B_4C in metallic foams coded a)66-b-2-B, b)66-b-4-B, and c)66-b-10-B.

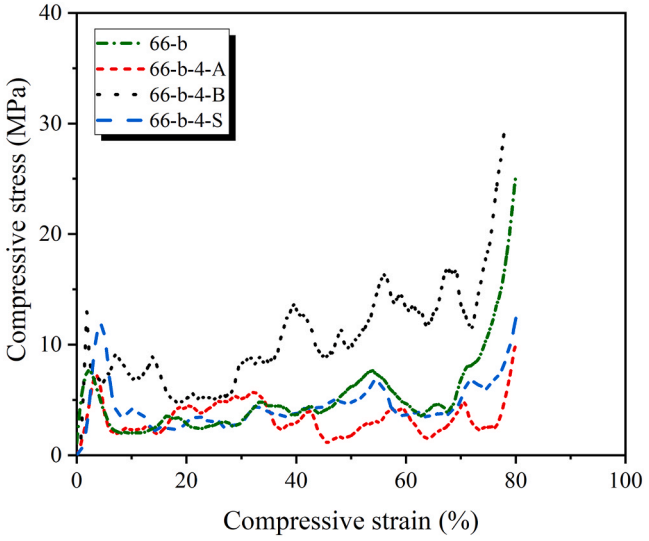

Fig. 12. Compressive stress-compressive strain of ceramic particle added open-cell aluminum foam.

Table 4
Comparison of properties of different Al foams.

Metal matrix	Porosity (%)	Pore size (mm)	Yield stress (MPa)	Densification Strain	Ref
Al-Si	85–90	1.5–2.5	2–4	0.4–0.5	[68]
Al−12Si	80–85	2–3	3–5	0.35–0.45	[69]
Al-Mg	75–85	1–2	1.5–3	0.45–0.55	[70]
Al-Cu	70–80	2.5–3.5	2.5–4.5	0.5–0.6	[29]
Al	38.59–74.97		2–9	0.2–0.6	[56]
Al	65.3–73.7	2–4.7			[46]
Al	25.51–26.47	1–2.4	60–80	0.7–0.8	Current paper
Al	80.92–81.88	1–2.4	1–1.5	0.8–0.85	Current paper

- The compressive strength and specific energy decreased with increasing porosity.
- According to compressive stress, the optimum ceramic ratio and type was determined as 4 % wt B_4C.

CRediT authorship contribution statement

Zafer Gölbaşı: Writing – review & editing, Writing – original draft, Software, Investigation, Formal analysis. **Bülent Öztürk:** Writing – review & editing, Writing – original draft, Supervision. **Nuray Beköz**

Üllen: Writing – review & editing, Writing – original draft.

Declaration of Competing Interest

The authors declare that they have no known competing financial interests or personal relationships that could have appeared to influence the work reported in this paper.

Acknowledgments

This work was supported by the Office of Scientific Research Projects of Karadeniz Technical University Project number: FDK-2018–7363.

Data availability

Data will be made available on request.

References

[1] H. Jain, G. Gupta, D.P. Mondal, A.K. Srivastava, A. Pandey, Sk Srivastava, R. Kumar, Effect of particle shape on microstructure and compressive response of 316L SS foam by space holder technique, Mater. Chem. Phys. 271 (2021).
[2] S. Sathaiah, R. Dubey, A. Pandey, N.R. Gorhe, T.C. Joshi, V. Chilla, D. Muchhala, D. P. Mondal, Effect of spherical and cubical space holders on the microstructural characteristics and its consequences on mechanical and thermal properties of open-cell aluminum foam, Mater. Chem. Phys. 273 (2021).
[3] B. Yang, R. Zhang, Z. Gao, X. Yu, Effect of nanoparticles and metal foams on heat transfer properties of PCMs, Int. J. Therm. Sci. 179 (2022).
[4] Z. Zhang, N. Liu, Z. Zhang, X. Xia, Z. Wang, J. Ding, J. Wang, Y. Liu, Compression performances of composite aluminum foam tubes, Int. J. Mech. Sci. 242 (2023).
[5] F.Ç. Durmus, L.P. Maiorano, J.M. Molina, Open-cell aluminum foams with bimodal pore size distributions for emerging thermal management applications, Int. J. Heat. Mass Transf. 191 (2022).
[6] S. Singh, N. Bhatnagar, A survey of fabrication and application of metallic foams (1925–2017), J. Porous Mater. 25 (2018) 537–554.
[7] C.Y. Zhao, Review on thermal transport in high porosity cellular metal foams with open cells, Int. J. Heat. Mass Transf. 55 (2012) 3618–3632.
[8] A.M. Harte, N.A. Fleck, M.F. Ashby, Fatigue failure of an open cell and a closed cell aluminium alloy foam, Acta Mater. 47 (1999) 2511–2524.
[9] R. Karuppasamy, D. Barik, Production methods of aluminium foam: A brief review, Mater. Today.: Proc. 37 (2021) 1584–1587.
[10] G. Yuan, Y. Li, X. Zhou, L. Hu, Preparation of complex shaped aluminum foam by a novel casting-foaming method, Mater. Lett. 293 (2021).
[11] O. Tripathi, D.P. Singh, V.K. Dwivedi, M. Agarwal, A focused review on aluminum metallic foam: Processing, properties, and applications, Mater. Today.: Proc. 47 (2021) 6622–6627.
[12] A.M. Medina Ramirez, R.R. Vintila, R.A.L. Drew, Morphology of aluminum alloy foams produced with dolomite via partial sintering of precursors, Materials 12 (2019).
[13] E. Shirjang, M.R. Akbarpour, Influence of severe plastic deformation of Cu powder and space holder content on microstructure, thermal and mechanical properties of copper foams fabricated by lost carbonate sintering method, J. Mater. Res. Technol. 26 (2023) 5437–5449.
[14] N. Kumar, A. Bharti, D. Prasad, M. Verma, A. Kumar Chauhan, Investigations on physical and mechanical properties of Mg composites and foams fabricated by powder metallurgy using NaCl, Mater. Today.: Proc. 78 (2023) 7–11.
[15] S.F. Aida, H. Zuhailawati, A.S. Anasyida, The Effect of Space Holder Content and Sintering Temperature of Magnesium Foam on Microstructural and Properties Prepared by Sintering Dissolution Process (SDP) Using Carbamide Space Holder, Procedia Eng. 184 (2017) 290–297.
[16] H. Jain, G. Gupta, R. Kumar, D.P. Mondal, Microstructure and compressive deformation behavior of SS foam made through evaporation of urea as space holder, Mater. Chem. Phys. 223 (2019) 737–744.
[17] J. Jakubowicz, G. Adamek, K. Pałka, D. Andrzejewski, Micro-CT analysis and mechanical properties of Ti spherical and polyhedral void composites made with saccharose as a space holder material, Mater. Charact. 100 (2015) 13–20.
[18] D.P. Mondal, M. Patel, H. Jain, A.K. Jha, S. Das, R. Dasgupta, The effect of the particle shape and strain rate on microstructure and compressive deformation response of pure Ti-foam made using acrowax as space holder, Mater. Sci. Eng.: A 625 (2015) 331–342.
[19] M. Dp, B. Ak, D. V, Effect of Strain Rate and Relative Density on the Compressive Deformation of Open Cell Ti6Al Alloy Foam through P/M Route, J. Appl. Mech. Eng. 06 (2017).
[20] A. Mansourighasri, N. Muhamad, A.B. Sulong, Processing titanium foams using tapioca starch as a space holder, J. Mater. Process. Technol. 212 (2012) 83–89.
[21] T. Um, S.K. Wilke, H. Choe, D.C. Dunand, Effects of pore morphology on the cyclical oxidation/reduction of iron foams created via camphene-based freeze casting, J. Alloy. Compd. 845 (2020) 156278.
[22] J. Pinto, D. Morselli, V. Bernardo, B. Notario, D. Fragouli, M.A. Rodriguez-Perez, A. Athanassiou, Nanoporous PMMA foams with templated pore size obtained by localized in situ synthesis of nanoparticles and CO2 foaming, Polymer 124 (2017) 176–185.
[23] T. Wan, Y. Liu, C. Zhou, X. Chen, Y. Li, Fabrication, properties, and applications of open-cell aluminum foams: a review, J. Mater. Sci. Technol. 62 (2021) 11–24.
[24] Y. Wang, H. Huang, G. Jia, G. Ke, J. Zhang, G. Yuan, Effect of grain size on the mechanical properties of Mg foams, J. Mater. Sci. Technol. 58 (2020) 46–54.
[25] J.A. Liu, S.J. Liu, B. Wang, W.B. Sun, X.J. Liu, Z.W. Han, Compressive property and energy absorption characteristic of interconnected porous Mg-Zn-Y alloys with adjusting Y addition, J. Magnes. Alloy. 12 (2024) 171–185.
[26] N. Jha, D.P. Mondal, J.Dutta Majumdar, A. Badkul, A.K. Jha, A.K. Khare, Highly porous open cell Ti-foam using NaCl as temporary space holder through powder metallurgy route, Mater. Des. 47 (2013) 810–819.
[27] D. Wang, X. Zhang, G. Zu, A. Qiao, Y. He, Y. Mu, Compressive properties of biomedical open-cell Zn foam, Mater. Res. Express 6 (2019) 115406.
[28] J. Liu, S. Liu, S. Shi, Z. Dong, D. Song, X. Zhu, Z. Han, Adjusting compressive properties of open-cell Mg-Gd-Zn foams by variation of Gd content, Mater. Sci. Eng.: A 820 (2021) 141562.
[29] M. Ashby, A. Evans, N. Fleck, L. Gibson, J. Hutchinson, H.N.G. Wadley, Metal Foams: a Design Guide, Mater. Des. 23 (2002) 119.
[30] K. Liu, C. Chen, W. Guo, B. Liu, B. Yang, Z. Li, J. Li, X. Li, F. Yin, Energy absorption and deformation behavior of multilayer aluminum foam structures, Mater. Sci. Eng.: A 832 (2022).
[31] B. Parveez, N.A. Jamal, A. Maleque, F. Yusof, N.H. Jamadon, S. Adzila, Review on advances in porous Al composites and the possible way forward, J. Mater. Res. Technol. 14 (2021) 2017–2038.
[32] T.R. Neu, P.H. Kamm, N. von der Eltz, H.-W. Seeliger, J. Banhart, F. García-Moreno, Correlation between foam structure and mechanical performance of aluminium foam sandwich panels, Mater. Sci. Eng.: A 800 (2021).
[33] B. Parveez, N.A. Jamal, H. Anuar, Y. Ahmad, A. Aabid, M. Baig, Microstructure and mechanical properties of metal foams fabricated via melt foaming and powder metallurgy technique: a review, Materials (2022).
[34] M. Bhuvanesh, G. Costanza, M.E. Tata, Research progress on mechanical behavior of closed-cell Al foams influenced by different TiH2 and SiC additions and correlation porosity-mechanical properties, : Appl. Sci. (2023).
[35] A. Hassani, A. Habibolahzadeh, H. Bafti, Production of graded aluminum foams via powder space holder technique, Mater. Des. 40 (2012) 510–515.
[36] J.H. Cadena, I.A. Figueroa, M.A. Suarez, O. Novelo-Peralta, G. González, G. Lara-Rodríguez, I. Alfonso, Production of Al foams using the SDP method: processing parameters and introduction a new sintering device, J. Min. Metall., Sect. B: Metall. 52 (2016) 47–52.
[37] F. Hassanli, M.H. Paydar, Improvement in energy absorption properties of aluminum foams by designing pore-density distribution, J. Mater. Res. Technol. 14 (2021) 609–619.
[38] Y. Li, J. Xiong, J. Lin, M. Forrest, P. Hodgson, C. Wen, Mechanical properties and energy absorption of ceramic particulate and resin-impregnation reinforced aluminium foams, Mater. Forum 31 (2007) 52–56.
[39] M.R. Moradi, A. Moloodi, A. Habibolahzadeh, Fabrication of nano-composite Al-B4C foam via powder metallurgy-space holder technique, Procedia Mater. Sci. 11 (2015) 553–559.
[40] M. Alizadeh, M. Mirzaei-Aliabadi, Compressive properties and energy absorption behavior of Al–Al2O3 composite foam synthesized by space-holder technique, Mater. Des. 35 (2012) 419–424.
[41] H. Farroukh, F. Kaddah, T. Wehbe, Numerical investigation of the optimal porosity of titanium foam for dental implants, Heliyon 10 (2024) e28063.
[42] N. Tuncer, G. Arslan, E. Maire, L. Salvo, Investigation of spacer size effect on architecture and mechanical properties of porous titanium, Mater. Sci. Eng.: A 530 (2011) 633–642.
[43] H. Bafti, A. Habibolahzadeh, Production of aluminum foam by spherical carbamide space holder technique-processing parameters, Mater. Des. 31 (2010) 4122–4129.
[44] B. Jiang, N.Q. Zhao, C.S. Shi, X.W. Du, J.J. Li, H.C. Man, A novel method for making open cell aluminum foams by powder sintering process, Mater. Lett. 59 (2005) 3333–3336.
[45] H. Bafti, A. Habibolahzadeh, Compressive properties of aluminum foam produced by powder-Carbamide spacer route, Mater. Des. 52 (2013) 404–411.
[46] S. Báez–Pimiento, M.E. Hernández–Rojas, M.E. Palomar–Pardavé, Processing and characterization of open–cell aluminum foams obtained through infiltration processes, Procedia Mater. Sci. 9 (2015) 54–61.
[47] W. Niu, C. Bai, G. Qiu, Q. Wang, Processing and properties of porous titanium using space holder technique, Mater. Sci. Eng.: A 506 (2009) 148–151.
[48] N. Bekoz, E. Oktay, Effects of carbamide shape and content on processing and properties of steel foams, J. Mater. Process. Technol. 212 (2012) 2109–2116.
[49] R.M. German, Powder Metallurgy and Particulate Materials Processing: the Processes, Materials, Products, Properties and Applications, Metal Powder Industries Federation, Princeton, New Jersey, 2005.
[50] A. Manonukul, N. Muenya, F. Léaux, S. Amaranan, Effects of replacing metal powder with powder space holder on metal foam produced by metal injection moulding, J. Mater. Process. Technol. 210 (2010) 529–535.
[51] A.C. Kaya, C. Fleck, Deformation behavior of open-cell stainless steel foams, Mater. Sci. Eng.: A 615 (2014) 447–456.
[52] N. Bekoz, E. Oktay, The role of pore wall microstructure and micropores on the mechanical properties of Cu–Ni–Mo based steel foams, Mater. Sci. Eng.: A 612 (2014) 387–397.
[53] I. Mutlu, E. Oktay, Mechanical properties of sinter-hardened Cr–Si–Ni–Mo based steel foam, Mater. Des. 44 (2013) 274–282.

[54] G. Kotan, Bor, Production and characterization of high porosity Ti-6Al-4V foam by space holder technique in powder metallurgy, Turk. J. Eng. Environ. Sci. 31 (2007).
[55] N.B. Ullen, Characterization of machinability of sintered steel foams having different porosities during drilling operations, Mach. Sci. Technol. 25 (2020) 527–557.
[56] A.Ahmad Hamdi, N.A. Mohd Sharif, A.Abu Seman, Dissolution method of aluminum foams containing Mg using carbamide space holder, Mater. Sci. Forum 888 (2017) 373–376.
[57] W.D. Callister, D.G. Rethwisch, Materials Science and Engineering: an Introduction, Wiley, 2014.
[58] N. Michailidis, F. Stergioudi, A. Tsouknidas, Deformation and energy absorption properties of powder-metallurgy produced Al foams, Mater. Sci. Eng.: A 528 (2011) 7222–7227.
[59] L.J. Gibson, M.F. Ashby. Cellular Solids: Structure and Properties, 2 ed., Cambridge University Press, Cambridge, 1997.
[60] G.E. Totten, D.S. Mackenzie, Handbook of Aluminum: Vol. 1: Physical Metallurgy and Processes, in, 2003.
[61] V. Sharma, N. Grujovic, F. Zivic, V. Slavkovic, Influence of Porosity on the Mechanical Behavior during Uniaxial Compressive Testing on Voronoi-Based Open-Cell Aluminium Foam, 12 (2019) 1041.
[62] K.M. Shorowordi, T. Laoui, A.S.M.A. Haseeb, J.P. Celis, L. Froyen, Microstructure and interface characteristics of B4C, SiC and Al2O3 reinforced Al matrix composites: a comparative study, J. Mater. Process. Technol. 142 (2003) 738–743.
[63] R. Yakut, N. Ürkmez Taşkın, Production of AA5754/B4C composite materials by the semi-solid stirring method, Technol. Appl. Sci. 14 (2019) 57–67.
[64] K. Halil, O. İsmail, D. Sibel, Ç. Ramazan, Wear and mechanical properties of Al6061/SiC/B4C hybrid composites produced with powder metallurgy, J. Mater. Res. Technol. 8 (2019) 5348–5361.
[65] T.J.A. Doel, P. Bowen, Tensile properties of particulate-reinforced metal matrix composites, Compos. Part A: Appl. Sci. Manuf. 27 (1996) 655–665.
[66] Ş. Karabulut, H. Karakoç, M. Bilgin, H. Canpolat, G.M. Krolczyk, M. Sarıkaya, A comparative study on mechanical and ballistic performance of functionally graded Al6061 composites reinforced with B4C, SiC, and Al2O3, J. Mater. Res. Technol. 23 (2023) 5050–5065.
[67] J. Banhart, Manufacture, characterisation and application of cellular metals and metal foams, Prog. Mater. Sci. 46 (2001) 559–632.
[68] V.C. Srivastava, K.L. SahooMetallic Foams: Current Status and Future Prospects, in, 2006. .
[69] H.N.G. Wadley, N. Fleck, A. Evans, Fabrication and Structural Performance of Periodic Cellular Metal Sandwich Structures, Compos. Sci. Technol. 63 (2003) 2331–2343.
[70] L. Gibson, Mechanical behavior of metallic foams, Annu. Rev. Mater. Sci. 30 (2000) 191–227.